POLITECNICO DI TORINO
Repository ISTITUZIONALE

Towards multi-body analyses for advanced flexible robotic systems

Original
Towards multi-body analyses for advanced flexible robotic systems / D'Imperio, Mariapaola; Canali, Carlo; Caldwell, Darwin; Cannella, Ferdinando; Pizzamiglio, Cristiano; Ludovico, Daniele; Mentrasti, Lando. - ELETTRONICO. - 9:(2017), p. V009T07A052. ((Intervento presentato al convegno ASME 2017 International Design Engineering Technical Conferences and Computers and Information in Engineering Conference, IDETC/CIE 2017 tenutosi a usa nel 2017 [10.1115/DETC2017-68095].

Availability:
This version is available at: 11583/2697666 since: 2018-01-17T15:05:24Z

Publisher:
American Society of Mechanical Engineers (ASME)

Published
DOI:10.1115/DETC2017-68095

Terms of use:
openAccess

This article is made available under terms and conditions as specified in the corresponding bibliographic description in the repository

Publisher copyright
IEEE postprint/Author's Accepted Manuscript

©2017 IEEE. Personal use of this material is permitted. Permission from IEEE must be obtained for all other uses, in any current or future media, including reprinting/republishing this material for advertising or promotional purposes, creating new collecting works, for resale or lists, or reuse of any copyrighted component of this work in other works.

(Article begins on next page)

08 November 2022

Towards multi-body analyses for advanced flexible robotic systems

Mariapaola D'Imperio[1], Cristiano Pizzamiglio[2], Daniele Ludovico[2], Lando Mentrasti[3], Carlo Canali[1], Darwin Caldwell[1] and Ferdinando Cannella[1]

***Abstract*— Manufacturers answered to the global competition rise by increasing the efficiency of their development process by substituing the hardware tests with their virtual counterpart. Following the same idea, in this paper, the introduction of the virtual prototyping technique in the design of a complex robotic leg is proposed. The novelty of this work is double: the first motivation lies on the characteristic of the mechanism, since it is a FLEXible jumping LEG; the second one, instead, regards to the introduction of methods well known in other research field but rarely used in robotics. This paper describes the whole design process, while the assembly of the physical prototype, the control development and the experimental tests will be matters of future works.**

I. INTRODUCTION

The rise of the global competition pushed the manufacturers to develop new products in less time then in the past and to improve their quality. These goals were reached by replacing the hardware tests with their virtual counterpart, namely the Multi-Body Models (MBMs). A MBM permits to study the motion analysis of a mechanical system, whether simple or complex. Several examples, related to the use of MBM to improve the products performances, can be found in the industrial research, such as the suspension in the automotive world, the landing gears in the aircraft industries and many others.

Following the same philosophy, the use of MBMs is here proposed for the robotic research where, even if the challenge is not related to the developing time spent in the design of a new robot, but to the desired performances, the integrated approach proposed by the MBMs strategy permits to overpass several limits of the traditional development process. In other words, it enables to perform a large variety of simulations for testing rapidly an efficiently several robot configurations in different operating scenarios, increasing the overall system performance at an early stage of the design process, hence reducing the number of experimental tests and avoiding costly design errors [1].

Nowadays the challenges that the robotic researches have to deal with are quite different: from the request of high precision movements in a narrow and delicate environment such as the human body [2] to the human-robotic interaction [3]; from the deep learning [4] to the choice of the optimum locomotion system [5]; from the request of having perfectly integrated prostheses to the high dynamic performances [6] such as jumping, running in case of legged robots. To the best of our knowledge, the panorama of the last family here mentioned can be represented by robot such as Mowgli [7], StarlETH [8], MSUJ Jumper [9], Bionic Kangoroo [10], MIT Cheetah 2 [11], GOAT [12], SALTO [6] and many others.

Mowgli is a jumping bipedal robot, it weights 30 N and it is able to jump more than 50% of its body height and it can land softly. StarETH is a compliant quadrupedal robot focused on fast, efficient, and versatile locomotion able to jump up to 150% of the leg length and it is also able to clear a gap of 0.23 m using a long jump. MSU Jumper is a mono-actuated miniature jumping robot that can perform a continuous steerable jumping based on the self-righting and the steering capabilities. The BionicKangaroo developed by Festo can recover the energy when jumping, store it and efficiently use it for the next jump. MIT Cheetah 2 is a quadrupedal robot able to autonomously detect and jump over obstacles up to 0.4 m as it runs at 2.5 m/s. The Gearless Omni-directional Acceleration vectoring Topology (GOAT) is an electro-mechanically actuated robot with legs capable of dexterous walking, running, and most significantly, explosive omni-directional jumping up to 0.82 m. The younger one, of this list, is the SAltatorial Locomotion on Terrain Obstacles, it is a one-legged hopper with the highest robotic vertical jumping agility ever recorded. It can jump 1 m high in a single leap.

Despite the high dynamic performances and the complex architecture of the aforementioned robots, none of the cited examples has a flexible structure. Here comes the double novelty of this work: from one side it describes the design process of a newly conceived robotic leg with flexible structural components, from the other side it shows how to implement the MBMs technique in the robotic research area. Designing robots by creating ad hoc and reliable codes would be too time consuming, especially when it is required to take into account for the flexibility of system's components undergoing large deformations. In the present paper, the mechanical configurations and the control algorithms of the FLEGX robotic limb were designed and simulated using the MSC.Nastran® and MSC.Adams®-Matlab/Simulink® integrated environment. Based on the Eulerian and Lagrangian dynamics, the MSC.Adams® code was successfully employed for the development of a reliable and detailed virtual prototype of the flexible leg.

[1]Mariapaola D'Imperio, Carlo Canali, Darwin Caldwell and Ferdinando Cannella are with the ADVR, Advanced Robotics Department of Istituto Italiano di Tecnologia, Genoa, Italy. {mariapaola.dimperio carlo.canali darwin.caldwell ferdinando.cannella}@iit.it

[2] Cristiano Pizzamiglio and Daniele Ludovico are with the DIMEAS, Department of Mechanical and Aerospace Engineering at Politecnico di Torino, Turin, Italy. cristiano.pizzamiglio@polito.it, daniele.ludovico@studenti.polito.it

[3]Lando Mentrasti is with DICEA, Deparment of Civil Engineering, Construction and Architecture, Universit Politecnica delle Marche, Ancona, Italy. mentrasti@univpm.it

The rest of the paper is organized as follows. Section II describes the mechanism, Section III details the different Multi-Body Models, in Section IV the performed simulations are discussed while Section V illustrates the paper results and concludes the paper.

II. Mechanism Description

FLEGX kinematic chain is composed by two subassemblies, namely the upperleg and the lowerleg, linked to each other by two revolute joints, namely the hip and the knee. The leg is connected to the external environment by a vertical linear guide . The latter consists of a thin rectangular carbon fibre plate, which slides on two supported shafts by means of four SKF® self-aligning linear bearing units with open housing. The robotic leg is coupled to the linear guide so that its plane of symmetry is coincident with the vertical plane of symmetry of the linear guide plate (Fig. 1.a).

The upperleg features a biologically inspired mechanical configuration and was conceived as rigid. It consists of a commercial round thin-wall aluminum tube having an outer diameter of 75mm, inner diameter equal to 71mm and a length of 180mm. The round tube features several holes with the purpose of lightening the structure: the resulting mass of the tube is approximately equal to 165g. Despite the high mass of the linear subsystem this solution presents a good torsional/axial stiffness and low mass and moments of inertia of the rigid segment and, in addition, has the advantage of being composed by several commercial parts.

The lowerleg, instead, is a straight flexible spring steel (AISI 304 - EN 1.4301) link having constant rectangular cross-section. As will be explained in detail later, a wide set of link geometries were studied; after these analyses, the following six links were built, where L, W, t are the length, width and thickness of the link respectively (in millimeters): Case 1 -200,50,3; Case 2 - 250,70,3; Case 3 - 250,50,3; Case 4 - 250,70,2; Case 5 - 250,50,2; Case 6 - 300,50,3.

FLEGX design was also focused on the reduction of the system inertia. It was obtained by locating the actuation system, composed by two brushless DC motors with two gearheads, on the linear guide supporting plate. With the aim of lowering the loads acting on the actuators during the jumping and landing phases, worm drives, with a 9.67:1 gear ratio, are employed as shown in Fig. 1.g. In order to transmit the motion at the knee joint, then, a floating worm wheel is employed: the hole of the wheel is drilled out allowing a deep groove double row ball bearing to be coupled with it; in turn, the inner ring of the ball bearing is constrained to the hip joint shaft, resulting in decoupling the motion of the hip and knee worm wheels. Eventually, a tendon-like system transfers the motion from the worm wheel to the knee joint. The two 266mm-long tendons are steel rods having a diameter of 7mm and a 10mm-long thread at both ends; they are linked to the worm gear and to the knee joint flange by means of spherical bearings (Fig. 1).

III. Multi Body Models

FLEGX final configuration derives from an extended optimization campaign focused on two objectives: lowering both masses and inertias and, at the same time, increasing the dynamic capabilities of the system, i.e. the jumping height. The virtual prototyping techniques played a key role in the identification of the optimal geometric and dynamic features of the system, such as the length and thickness of the flexible link or the inertial properties of the whole assembly, and in the choice of the most suitable mechanical and electromechanical components. The simulations were performed using the software MSC.Nastran® and MSC.Adams®-Matlab/Simulink® integrated environment.

Three different virtual models were developed. The simpler one, the Pseudo-Rigid-Body Model (PRBM), which features a lumped flexible component, was thought as a preliminary tool for studying efficiently several geometries of the flexible link with the aim of identifying a smaller set of geometries to be used for the subsequent and more detailed analyses. The second one, called Linear Flexible Model (LFM), more sophisticated with respect to the PRBM, contains the flexible component modelled in a proper Finite Element environment. It was built to verify that the lowerleg stresses were lower than the ultimate tensile strength of the link material, namely between 510 and 530MPa (Von Mises criterion). In the most complex model, the efficiency of the actuation system was tested: it is called Machinery Model (MM). In all the models the upperleg, the tendons and the vertical guide were modelled as rigid components. The connection between the upperleg and the vertical guide (Fig. 1.a) was modelled as a translational joint whereas the two internal connections in the PRBM and LFM were modelled as ideal revolute joints. In all the cases, with the aim of reducing the solution time and avoiding solver issues during the simulations with the LFM, the contact between the flexible link and the ground was not directly modelled; indeed, the interaction between the ground and a rigid cylinder having negligible mass, constrained by a fixed joint to the lower interface node of the flexible link, was implemented. That choice permitted to model the contact between two rigid bodies by using the Impact-Function-Based algorithm that implements a nonlinear spring damper element.

A. Pseudo-Rigid-Body Model

The Pseudo-Rigid-Body Model (PRBM) of the flexible link was developed on the basis of the fundamental works by Howell and Midha [13]–[17]. As stated in [16], the PRBM is a simple method successfully used in the design and kinetostatic analysis of compliant mechanisms; by applying the mechanics of rigid bodies, it allows to simplify the large-deflection non-linear analyses of flexible structures.
The classical PRB 1R model was adopted, where R stands for a revolute joint. As displayed in Fig. 1.c, the lower link was modelled as a cantilever beam consisting of two rigid body links joined together at the pin joint, also called characteristic pivot. With the aim of modelling the beam compliance, a

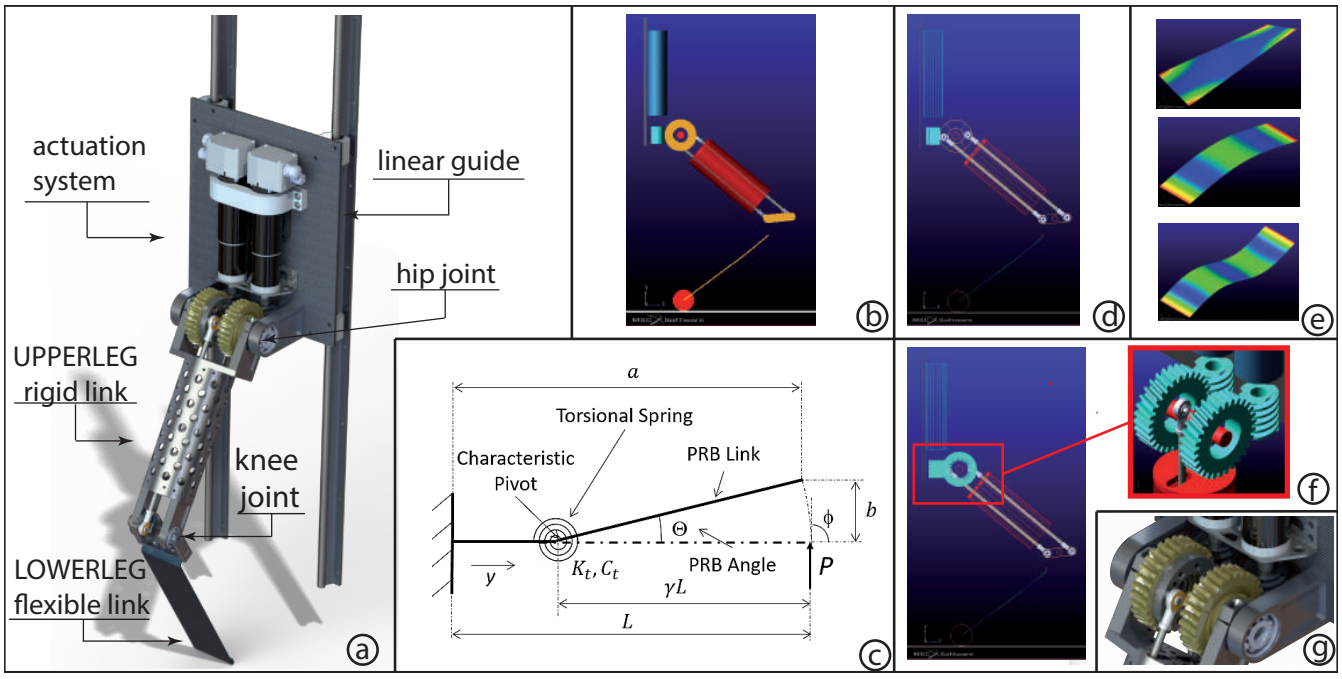

Fig. 1. a) FLEXible LEG mechanical design; b) FLEGX Pseudo Rigid Body Model; c) Pseudo Rigid Body Model theoretical schema; d) FLEGX Linear Flexible Model; e) Three modeshapes of the flexible component obtained with the .mnf file; f) FLEGX Machinery Model; g) Worm gear details.

torsion spring of equivalent stiffness K_t is located at the pin joint, whose position is governed by the characteristic radius factor γ. The latter, as described in [18] and in [17], is estimated through an optimization procedure such that the PRB characteristic length γL, where L is the continuum beam total length, will trace a path within a defined error of 0.5% with respect to the corresponding closed-form elliptic integral solution for a cantilever beam. In particular, γ is equal to 0.852 for a vertical force [15], [17].
Defining θ_0 as the inclination of the beam in the deformed configuration, it is possible to find a parallelism with Θ, that is the PRB inclination, such as $\theta_0 = c_\theta \Theta$ [16].

Having said that, the coordinates of the beam end can be written as

$$\left[a/L; b/L\right] = \left[1 - \gamma(1 - cos(\Theta)); \gamma sin(\Theta)\right] \quad (1)$$

while the spring torsional stiffness can be estimated by [16]

$$K_t = \gamma K_\theta EI/L \quad (2)$$

where K_θ is the beam stiffness coefficient, E is the Young Modulus of the material and I is area moment of inertia of the beam. For a vertical end force, c_θ and K_θ are approximately equal to 1.239 and 2.649 respectively [15], [17].

Since the FLEGX robotic limb has to perform a highly dynamic task, namely a vertical jump, the PRBM has to be modified in order to describe, not only the static, but also the dynamic behaviour of the flexible link. Articles like [16], [19] proved that the PRBM is also an effective tool for the dynamic modelling of compliant mechanisms. The PRBM for the dynamic analysis of the lower link was developed by imposing the equality between the undamped natural frequency of the latter and the first natural frequency of the continuum cantilever beam. As is well known, the lowest natural frequency ω_1, corresponding to a bending mode, for a continuous uniform cantilever beam can be computed by

$$\omega_1 = \frac{1.875^2}{L^2}\sqrt{\frac{EI}{\lambda}} \quad (3)$$

where λ is the linear mass density of the beam. For what concern the PRBM, the non-dimensional tangential load factor [17] can be written as:

$$\alpha_t^2 = \frac{P_t L^2}{EI} \quad (4)$$

where P_t is the tangential load given by

$$P_t = P\sin(\phi - \Theta). \quad (5)$$

Assuming that only a vertical non-follower end force P is acting, the angle ϕ, formed by the horizontal and the direction of the force vector, is equal to 90°, hence Eq. 5 becomes

$$P_t = P\sin(\phi - \Theta) = P\cos\Theta. \quad (6)$$

Moreover, it is possible to write the relationship [17]

$$\alpha_t^2 = K_\Theta \Theta. \quad (7)$$

By combining together Eqs. 1, 2, 4, 6 and 7, the following nonlinear equation is derived

$$\frac{\cos\left[\arcsin\left(\frac{b}{\gamma L}\right)\right]}{\arcsin\left(\frac{b}{\gamma L}\right)} = \frac{K_t}{\gamma PL}, \quad (8)$$

which can be numerically solved to compute the static vertical displacement of the beam end as function of K_t

and γ. Since it is a dynamic problem, it is also necessary to determine the damping coefficient C_t of the torsion spring. Hence, three parameters have to be computed, namely γ, K_t and C_t, in order to build a dynamic PRBM of the flexible link. According to the theory of the torsional harmonic oscillator, the undamped natural frequency f of the PRB link is equal to

$$f = \frac{\omega}{2\pi} = \frac{1}{2\pi}\sqrt{\frac{K_t}{J}} \tag{9}$$

where ω is the natural frequency expressed in $rad \cdot s^{-1}$ and J is the mass moment of inertia of the PRB link. By means of the Huygens-Steiner theorem, and remembering that the PRB link has a constant rectangular section, its mass moment of inertia is given by

$$J = \frac{\rho\gamma LWt}{3}\left[(\gamma L)^2 + \frac{t^2}{4}\right] \tag{10}$$

Finally, the damping ratio ξ is equal to

$$\xi = \frac{C_t}{2\sqrt{K_t J}} \tag{11}$$

Equations 8, 9 and 11 give rise to a system of nonlinear equations in three variables: γ, K_t and C_t. For instance, a 300mm long, 50mm wide and 3mm thick flexible link is consider. For this link the first natural frequency ω_1 is equal to

$$\omega_1 = 171.3194 rad/s = 27.2663 deg/s.$$

If P is equal 30N, the value of the vertical displacement b is approximately equal to $12mm$. The damping ratio was assumed equal to 0.015. By solving the aforementioned system of nonlinear equations, assuming proper initial guesses on the basis of the values given in [15], the following results for the three unknowns were obtained:

$$\gamma = 0.7377,$$

$$K_t = 2165.2 Nmm/deg, \quad C_t = 0.3792 Nmms/deg$$

and the mass moment of inertia of the PRB link was equal to 4226.8 $kgmm^2$. Then, in order to test the quality of the PRBM, two take-off analyses were carried of the FLEGX system in the MSC.Adams® environment. In the first analyses the robotic limb was equipped with the LFM of the link, while in the second one the PRBM of the link was implemented. These two simulations were carried out imposing the same motion laws for the hip and knee joints and the results were compared as shown in Fig. 3. It can be noticed, for example, that the PRBM approximates quite well the free-end displacement of the LFM. The robotic leg with the LFM reached a jumping height equal to 50 mm, while with the PRBM the jumping height was approximately equal to 60 mm. The PRBM is an analytical model based on while the LFM is a conceived by the numerical approach. For this reason, there are small differences during the results comparison, that can be tolerated.

B. Linear Flexible Model

In the linear flexible model (LFM) the lower link has been as an *.mnf* file. A modal neutral file (.mnf) is generated with a MSC.Nastran® and it contains information such as inertia matrix invariants, mode-shapes and frequencies of the modal base derived from fixed boundary eigenmodes through an orthonormalization procedure, namely the Craig-Bampton method [20]. This procedure is required to optimize the computational effort necessary to perform a dynamic simulation of flexible structures.

The description of a flexible component in a Finite Element software transforms the infinite number of DOF of the continuum in a finite, but very large, number of DOF of the discrete system. The system displacement u can be represented by a linear combination of mode shapes ϕ_i, such as

$$u = \sum_{i=1}^{M} \phi_i q_i = \Phi q \tag{12}$$

where M is the modeshapes number and q_i are the modal coordinates. Generally speaking, a static analyses require a larger number of DOF to map internal stresses and strain respect to a dynamic one that is based, mainly, on the knowledge of the system frequency. For these reasons, in order to reduce the computational effort of a flexible dynamic analysis, the aforementioned number of modeshapes has to be reduced. The system displacements (u) are partioned in boundary (u_B) and interior (u_I). The u_B are obtained by giving to them a unit displacement keeping the u_I fixed; the u_I instead, are calculated by fixing the u_B and computing an eigensolution. At the end, the relationship obtained is given by

$$u = \begin{bmatrix} u_B \\ u_I \end{bmatrix} = \begin{bmatrix} I, 0 \\ \Phi_{IC}, \Phi_{IN} \end{bmatrix} \begin{bmatrix} q_C \\ q_N \end{bmatrix} = \Phi \begin{bmatrix} q_C \\ q_N \end{bmatrix} \tag{13}$$

where Φ_{IC} represents the physical displacement of the u_I, Φ_{IN} are the physical displacement of the normal modes, q_C are the modal coordinates of the constraint modes while q_N are the modal coordinates of the fixed-boundary normal modes.

Thanks to this substitution is then possible to rewrite the system stiffness matrix as

$$\hat{K} = \Phi^T K \Phi = \Phi^T \begin{bmatrix} K_{BB}, K_{BI} \\ K_{IB}, K_{II} \end{bmatrix} \Phi = \begin{bmatrix} \hat{K}_{CC}, 0 \\ 0, \hat{K}_{NN} \end{bmatrix} \tag{14}$$

$$\hat{M} = \Phi^T M \Phi = \begin{bmatrix} \hat{M}_{CC}, \hat{M}_{NC} \\ \hat{M}_{CN}, \hat{M}_{NN} \end{bmatrix} \tag{15}$$

that results in $\hat{K}_{NN}$ and $\hat{M}_{NN}$ diagonal matrices, $\hat{K}$ is block diagonal because there is no coupling stiffness between the constraints modes and the fixed boundary ones; while $\hat{M}$ is not block diagonal because there is the inertia coupling between the constraint modes and the fixed-boundary ones.

TABLE I

RESULTS OF THE FIRST SET OF SIMULATIONS: SEARCH FOR THE OPTIMUM FLEGX MECHANICAL DESIGN.

Configuration	Total mass $[kg]$	Jump height $[mm]$	Max. stress $[MPa]$
No.1	8.77	70.88	522.90
No.2	9.57	59.80	523.62
No.3	7.35	108.1	514.62
No.4	7.97	104.1	530.68

C. Machinery Model

As stated above, the FLEGX system features a couple of right-hand worm gear sets. Worm gears efficiency, which typically ranges between 0.40 and 0.85 [21], depends on various factors, for instance, the lead angle, the gear ratio, the running speed and the lubrication conditions. The efficiency can be computed in the following way (worm driving) [22]:

$$\eta = \frac{\cos\vartheta_n - f\tan\alpha}{\cos\theta_n + (f/\tan\alpha)} \tag{16}$$

where f is the friction coefficient of the materials in contact, α is the worm lead angle and θ_n is the normal pressure angle given by

$$\tan\vartheta_n = \tan\vartheta\cos\alpha. \tag{17}$$

It is clear that the efficiency of the worm gears can significantly affect the overall performance of the robotic leg, thus a detailed study is needed.

Virtual prototypes of the worm gears were implemented, in the FLEGX multibody model (Fig. 1.g), using the MSC.Adams/Machinery® module. The 3D Contact algorithm was employed: it uses a geometry-based contact and is able to compute true backlash based on actual working center distance and tooth thickness [23].
Both worm gear sets are identical. The pressure angle is equal to $15°$, the module is 2.5 mmand the center distance is equal to 53 mm. The worms, made of case hardened steel, have three threads, while the worm wheels, which feature 29 teeth, are made of bronze (CuZn40Al2/So). If mineral grease is used as lubricant, worm wheels can bear an output torque equal to $77Nm$.

IV. SIMULATIONS

The above mentioned numerical models were tested in MSC.Adams®-Matlab/Simulink® integrated environment and/or in MSC.Nastran®. Two main groups of simulations were carried out: the first one aimed at finding the optimum FLEGX design, while the second one was focused on assessing the impact of the worm gear efficiency on the overall performance of the system.

In the *first group* of simulations four different upperleg configurations were tested.
The configuration No.1 (Fig. 2.a) was modelled as the HyQ [24] upperleg segment, with the actuation system directly coupled with the two joints; in the second one (Fig. 2.b), the upper leg consists of a commercial round aluminium tube having a 90 mm outer diameter and the two motors and gearheads were placed close to the hip joint with their longitudinal axis parallel to the one of the upper leg cylinder; the configuration No.3 (Fig. 2.c) features an aircraft semi-monocoque fuselage-like structure and the hip motor was placed directly on the linear guide support plate, whereas the knee joint actuator is mounted within the upper leg structure; in the forth configuration (Fig. 2.d), already described in the previous section, the actuation system was completely located on the linear guide support plate.

Fig. 2. Upperleg designs. a) Configuration N1, b) Configuration N2, c) Configuration N3, d) Configuration N4

For this first set of analyses, the investigated movement was the take-off phase. The simulations were run using the *GSTIFF* implicit predictor-corrector integrator and, with the aim of increasing the stability and robustness of the solver, the *SI2* (Stabilized Index 2) formulation was used. Usually, the *SI2* allows to avoid the very short-duration numerical spikes for velocities and accelerations. After several preliminary simulations the permissible solution convergence error was set to $1 \cdot 10^{-4}$.
The four mechanical configurations were equipped with a 250 mm long, 70 mm wide and 3 mm thick flexible link. The simulations were performed by requiring that the maximum value of the stresses in the lower link was sufficiently lower than the ultimate tensile strength of the link material, namely between 510 and 530MPa (Von Mises criterion). The take-off was performed by rotating the hip and the knee joints with proper motion laws as a function of time. The jumping technique (i.e. countermovement jump) can be described as follows: the robotic leg starts at a static standing position and then squats down in few seconds; then, the hip and knee joints rapidly rotate again, but in the opposite directions,

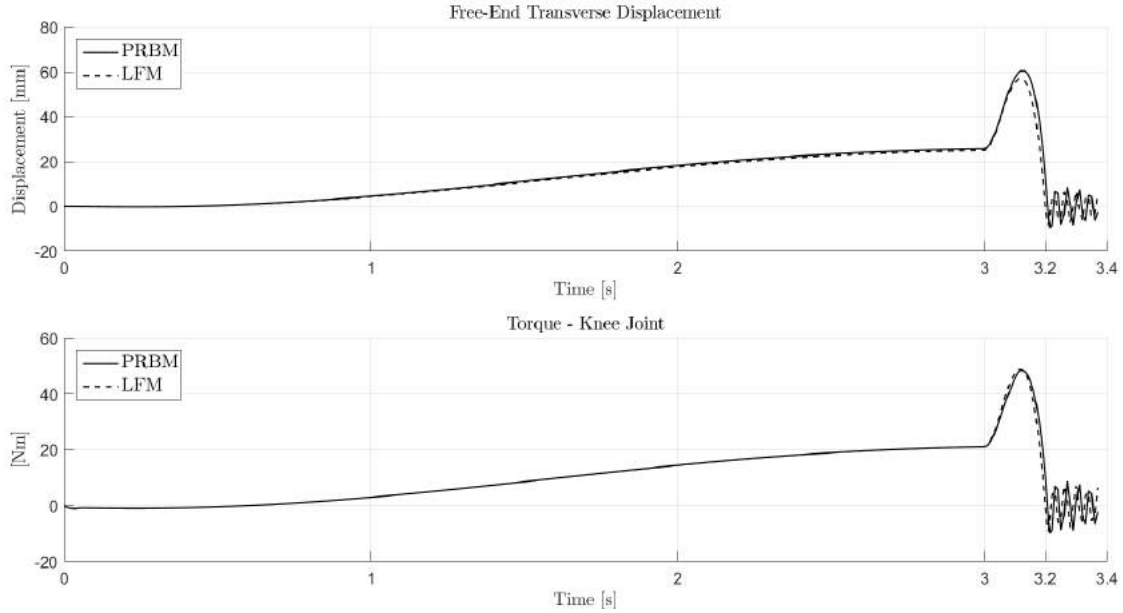

Fig. 3. Comparison between the PBRM and LFM in the estimation of free end transversal displacement and in the torques exerted at the knee joint in a jumping performances.

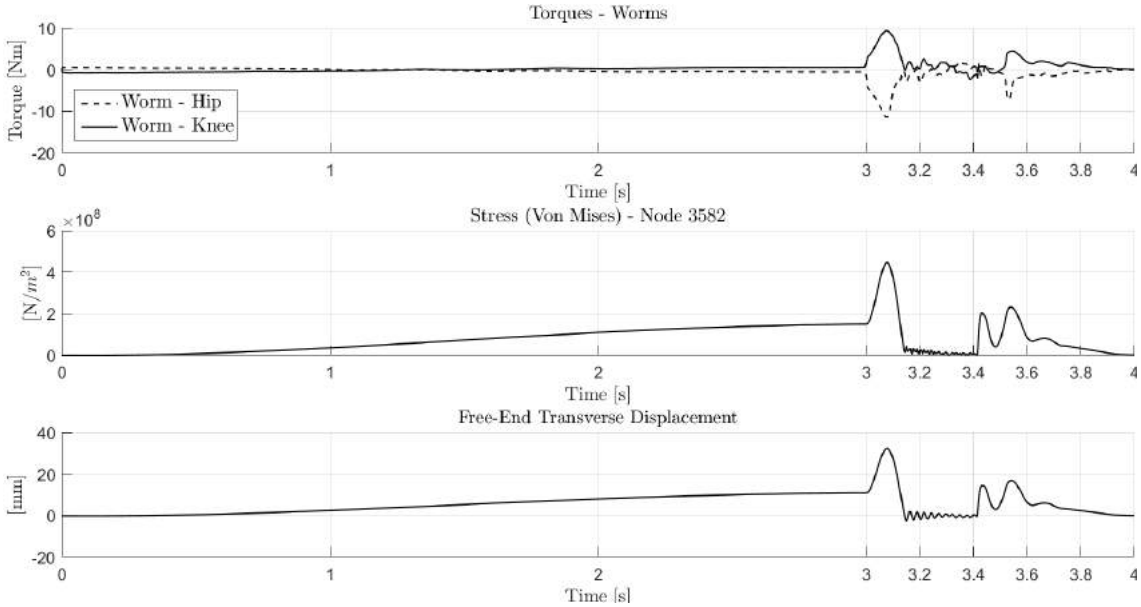

Fig. 4. Machinery model: the take-off and landing phases were analyzed. The lower link was 250 mm long, 70 mm wide and 3 mm thick. The first graph shows the torques required at the hip and knee worm in order to carry out a 50 mm jump. In the second plot is illustrated the evolution of the stresses at the fixed-end of the flexible link: the maximum stress recorded is equal to $447MPa$, a value definitely lower than the AISI 304 ultimate tensile strength. The free-end transverse displacement is displayed in the third figure: the maximum displacement is approximately equal to $32mm$, that is the 12.8% of the total length of the flexible link.

allowing the leg to jump vertically up off the ground. In order to avoid unwanted vibrations, the motions were described by a cubic polynomial function that approximates the Heaviside step function [1], such as

$$STEP = \begin{cases} \theta_0 : t \leq t_0 \\ \theta_0 - a\Delta^2(3 - 2\Delta) : t_0 < t \leq t_1 \\ \theta_1 : t \geq t_1 \end{cases} \tag{18}$$

with $a = (\theta_1 - \theta_0)$ and $\Delta = \frac{(t-t_0)}{(t_1-t_0)}$.

In the *second group* of simulations, a detailed virtual model of the worm gear sets was developed by employing the MSC.Adams/Machinery®module. Unlike the first set of analyses, these simulations were run using the the Hilber-Hughes-Taylor (HHT) integrator. As stated in [23], the HHT solver seems to offer the highest performance and stability, with respect to the GSTIFF integrator, when the Machinery module is used. The default error tolerance, equal to $1 \cdot 10^{-5}$,

was not modified. It was very difficult to determine realistic contact parameters for the worm gears; as a matter of fact, there is a lack of information in the literature for parameters like the stiffness or the dynamic friction transition velocity. Thus, several simulations were carried out in order to understand how a variation of these parameters could affect the overall behaviour of the system; however, a certain level of uncertainty still remained for the values of the damping coefficient, the static and dynamic friction transition velocities. The value of the static friction coefficient μ_s was determined in accordance with the information provided by the worm gear manufacturer: for the worm gear chosen, an efficiency equal to 0.64 was declared. However, considering that the starting efficiency is lower than the running efficiency and many other factors can reduce the efficiency of the worm gear, such as the sliding velocity and the temperature, a 0.60 efficiency was assumed. By using Eq. 16, the corresponding friction coefficient can be evaluated and it is approximately equal to 0.14; the dynamic static coefficient was then set equal to 0.13. In Fig. 4 the results of a 50 mm jump are displayed; both the take-off and landing phases were simulated.

V. Results and Conclusions

This results of the first group of simulations are collected in Tab. I and in Fig. 3 . For each case study the maximum jumping height reached, the maximum stresses developed in the flexible link, the total mass and the related inertia of the system are detailed. It may be observed that the solutions No.3 and No.4 shown the best performances with a jumping height of 108.1 and 104.1 mm respectively, thus the configurations No.1 and No.2 were discarded. With regard to the third configuration, it benefits from a very high torsional and axial stiffness of the upper leg segment and very low mass of the rigid segment, but its construction would require higher costs and would take longer time due to the fact that the rigid link parts aren't commercial components. According to these observations and bearing in mind the considerations outlined in section II, the solution No.4 was the selected one. The results of the second group of simulations, instead, are shown in Fig 4. A 50 mm jump with its take off and landing phases are described. The next steps are focused on the physical prototyping construction in order to perform several experimental tests to validate the aforementioned numerical model. A development of a proper control system, able to deal with a flexible robotic structure is also necessary. Furthermore, in a longer future, the evaluation of different shapes for the flexible link will be also considered and, at the same time, the analysis of its non-linear behaviour has to be investigated by proper ad hoc simulations.

References

[1] M. ADAMS and C. Documentation, "Msc," *Software Corporation*, 2005.

[2] I. A. Broeders, "Robotics: The next step?" *Best Practice & Research Clinical Gastroenterology*, vol. 28, no. 1, pp. 225–232, 2014.

[3] K. Kosuge and Y. Hirata, "Human-robot interaction," in *Robotics and Biomimetics, 2004. ROBIO 2004. IEEE International Conference on*. IEEE, 2004, pp. 8–11.

[4] Y. LeCun, Y. Bengio, and G. Hinton, "Deep learning," *Nature*, vol. 521, no. 7553, pp. 436–444, 2015.

[5] C. G. Atkeson, B. Babu, N. Banerjee, D. Berenson, C. Bove, X. Cui, M. DeDonato, R. Du, S. Feng, P. Franklin *et al.*, "No falls, no resets: Reliable humanoid behavior in the darpa robotics challenge," in *Humanoid Robots (Humanoids), 2015 IEEE-RAS 15th International Conference on*. IEEE, 2015, pp. 623–630.

[6] D. W. Haldane, M. Plecnik, J. Yim, and R. Fearing, "Robotic vertical jumping agility via series-elastic power modulation," *Science Robotics*, vol. 1, no. 1, p. eaag2048, 2016.

[7] R. Niiyama, A. Nagakubo, and Y. Kuniyoshi, "Mowgli: A bipedal jumping and landing robot with an artificial musculoskeletal system," in *Robotics and Automation, 2007 IEEE International Conference on*. IEEE, 2007, pp. 2546–2551.

[8] M. Hutter, C. Gehring, M. Bloesch, M. A. Hoepflinger, C. D. Remy, and R. Siegwart, "Starleth: A compliant quadrupedal robot for fast, efficient, and versatile locomotion," in *15th International Conference on Climbing and Walking Robot-CLAWAR 2012*, no. EPFL-CONF-181042, 2012.

[9] J. Zhao, J. Xu, B. Gao, N. Xi, F. J. Cintrón, M. W. Mutka, and L. Xiao, "Msu jumper: A single-motor-actuated miniature steerable jumping robot," *IEEE Transactions on Robotics*, vol. 29, no. 3, pp. 602–614, 2013.

[10] B. Jun, Y. Kim, and S. Jung, "Design and control of jumping mechanism for a kangaroo-inspired robot," in *Biomedical Robotics and Biomechatronics (BioRob), 2016 6th IEEE International Conference on*. IEEE, 2016, pp. 436–440.

[11] H.-W. Park and S. Kim, "Quadrupedal galloping control for a wide range of speed via vertical impulse scaling," *Bioinspiration & biomimetics*, vol. 10, no. 2, p. 025003, 2015.

[12] S. Kalouche, "Design for 3d agility and virtual compliance using proprioceptive force control in dynamic legged robots," Ph.D. dissertation, CARNEGIE MELLON UNIVERSITY, 2016.

[13] S. Lyon, P. Erickson, M. Evans, and L. Howell, "Prediction of the first modal frequency of compliant mechanisms using the pseudo-rigid-body model," *Journal of Mechanical Design*, vol. 121, no. 2, pp. 309–313, 1999.

[14] L. L. Howell, *Compliant mechanisms*. John Wiley & Sons, 2001.

[15] J. Pauly and A. Midha, "Improved pseudo-rigid-body model parameter values for end-force-loaded compliant beams," in *ASME 2004 International Design Engineering Technical Conferences and Computers and Information in Engineering Conference*. American Society of Mechanical Engineers, 2004, pp. 1513–1517.

[16] Y.-Q. Yu, L. L. Howell, C. Lusk, Y. Yue, and M.-G. He, "Dynamic modeling of compliant mechanisms based on the pseudo-rigid-body model," *Journal of Mechanical Design*, vol. 127, no. 4, pp. 760–765, 2005.

[17] R. S. Kuber, "Development of a methodology for pseudo-rigid-body models of compliant segments with inserts, and experimental validation," 2013.

[18] L. L. Howell, "The design and analysis of large-deflection members in compliant mechanisms," Ph.D. dissertation, 1991.

[19] L. Howell and A. Midha, "A loop-closure theory for the analysis and synthesis of compliant mechanisms," *TRANSACTIONS-AMERICAN SOCIETY OF MECHANICAL ENGINEERS JOURNAL OF MECHANICAL DESIGN*, vol. 118, pp. 121–125, 1996.

[20] J.-G. Kim and P.-S. Lee, "An enhanced craig–bampton method," *International Journal for Numerical Methods in Engineering*, vol. 103, no. 2, pp. 79–93, 2015.

[21] R. L. Norton, *Design of machinery: an introduction to the synthesis and analysis of mechanisms and machines*. McGraw-Hill Inc., US, 1999.

[22] G. Jacazio and S. P. Pastorelli, *Meccanica applicata alle macchine*. Levrotto & Bella Editore, 2001.

[23] M. Software, "Welcome to adams machinery," Tech. Rep., 2017.

[24] C. Semini, "Hyqdesign and development of a hydraulically actuated quadruped robot," *Doctor of Philosophy (Ph. D.), University of Genoa, Italy*, 2010.